ChemComm



FEATURE ARTICLE

View Article Online



Cite this: Chem. Commun., 2022, **58**. 8182

Strategies and characterization methods for achieving high performance PEO-based solidstate lithium-ion batteries

Bin Guo,†a Yanda Fu,†b Jianan Wang, o Yi Gong,d Yunlong Zhao, o Kai Yang,*d Sida Zhou, Lishuo Liu, * Shichun Yang, Xinhua Liu and Feng Pan *

Polyethylene oxide (PEO) based polymer electrolytes have been widely used in solid-state lithium batteries (SSBs) owing to the high solubility of lithium salt, favourable ionic conductivity, flexibility for improved interfacial contact and scalable processing. In this work, we summarize the main limitations remaining to be solved before the large-scale commercialization of PEO-based SSBs, including (1) improving ionic conductivity toward high-rate performance and lower operating temperature, (2) enhancing mechanical strength for improved lithium dendrite resistance and large-scale processing, (3) strengthening electrochemical stability to match high energy density electrodes with high voltage, and (4) achieving high thermal stability toward safe operation. Meanwhile, the characterization methods to investigate the ion transportation mechanism, lithium dendrite growth and decomposition reaction are also discussed.

Received 23rd April 2022, Accepted 14th June 2022

DOI: 10.1039/d2cc02306g

rsc.li/chemcomm

1. Introduction

With the ever-increasing demand for high energy/power density lithium-ion batteries (LIBs), great challenges have been put forward for conventional liquid LIBs. Lithium metal anodes, delivering the highest specific capacity (3860 mA h g⁻¹) and the lowest voltage (-3.04 V vs. SHE), have been regarded as next generation anodes with great commercial value.1 However, safety hazards are also introduced owing to the severe electrolyte decomposition and gas release, lithium dendrite growth and continuous heat generation, and even trigger the thermal runaway accompanied by smoke, fire and even explosion. 1,2 Solid state batteries (SSBs) employing solid-state electrolytes (SSEs) have been developed over the past decades to enhance lithium dendrite resistance and realize the utilization of lithium metal anodes.³ Various inorganic electrolytes including oxide, garnet, etc. have been reported to improve the long-term/

Lithium-ion mobility (across the interface and within the electrolyte), mechanical strength (mitigating lithium dendrite and flexibility for manufacture), and thermal/electrochemical stability are the key parameters for the practical application of polymer-based SSEs.^{7,8} The flexible molecular polyether segments of PEO coordinate with lithium ions via coulombic interaction to deliver lithium-ion conductivity. The coordination structure will dissociate under an electric field driving force and the thermal movement of PEO chains.9 Consequently, directional lithium ion migration is realized by the "coordination-dissociation" effect between ether oxygen atoms

high current density cycling of lithium metal SSBs. 4,5 Due to the rigid contact between solid electrolytes and active materials, a large interfacial resistance is created leading to a large overpotential for charge transfer.⁵ Meanwhile, solid electrolyte membranes using pure inorganic electrolytes are often millimetre-scale in thickness which will sacrifice the energy density and make it difficult for large-scale manufacturing.6 Solid polymer electrolytes with high flexibility/lithiumcompatibility have been regarded as a promising alternative for inorganic solid electrolytes. Among many polymer electrolyte systems, polyethylene oxide (PEO) is one of the most widely used polymers owing to its advantages of high solubility of lithium salt, easy-processing, low cost, and acceptable stability against lithium metal.8 Since its first demonstration as a solid electrolyte, PEO-based solid state batteries have received extensive attention and been widely developed with versatile prototypes as shown in Fig. 1.

^a School of Transportation Science and Engineering, Beihang University, Beijing, 100191, China

^b School of Advanced Materials, Peking University Shenzhen Graduate School, Shenzhen, 518055, China. E-mail: panfeng@pkusz.edu.cn

^c Department of Environmental Science and Engineering, School of Energy and Power Engineering, Xi'an Jiaotong University, Xi'an, 710049, China

^d Advanced Technology Institute, University of Surrey, Guildford, Surrey, GU2 7XH, UK. E-mail: kai.yang@surrey.ac.uk

^e State Key Laboratory of Automotive Safety and Engineering, Tsinghua University, Beijing, 10084, China, E-mail: liulishuo12@126.com

[†] These authors contributed equally to this work.

Feature Article ChemComm

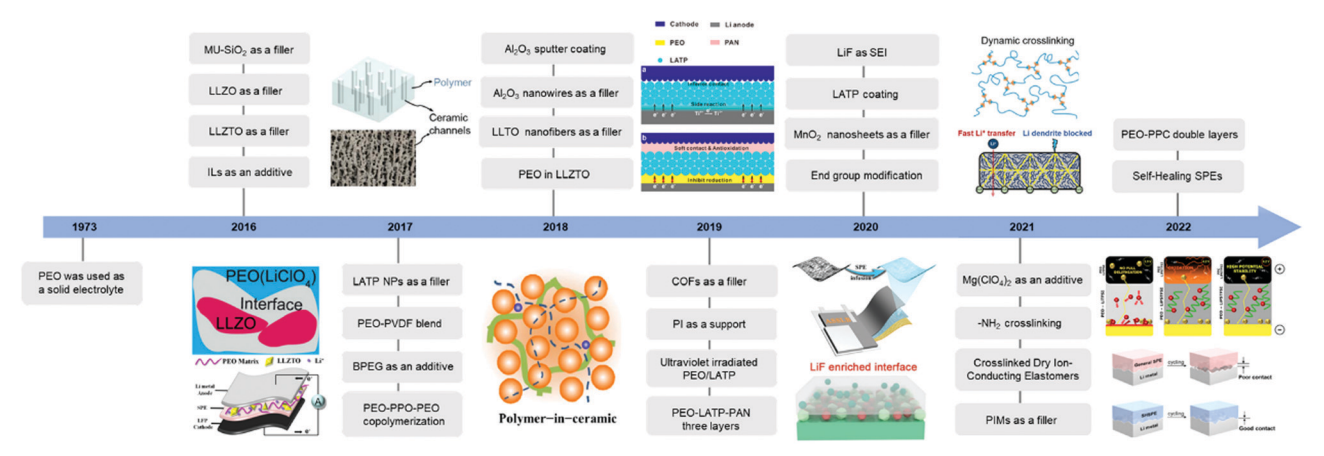


Fig. 1 A brief timeline of research progress in PEO-based solid state batteries. LLZO filler image.¹¹0 Reproduced with permission. Copyright⊚2016, WILEY-VCH Verlag GmbH & Co. Vertically aligned and connected $\text{Li}_{1+x}\text{Al}_x\text{Ti}_{2-x}(\text{PO}_4)_3$ (LATP) in the PEO matrix. Reproduced with permission. Copyright©2017, American Chemical Society. Polymer in the ceramic image. Reproduced with permission. Copyright©2017 Elsevier Ltd. Multilayer design image. 13 Reproduced with permission. Copyright © 2019 American Chemical Society. Li₂S acts as the filler. 14 Reproduced with permission. Copyright © 2020 WILEY-VCH Verlag GmbH & Co. Dynamically crosslinked PEO electrolytes. 15 Reproduced with permission. Copyright © 2021 Wiley-VCH GmbH. Self-healing PEO electrolytes. 16 Reproduced with permission. Copyright © 2021 American Chemical Society.

and lithium ions. An amorphous region is reported to dominate the lithium conductivity of PEO. At room temperature, PEO possess high crystallinity and poor chain movement ability, resulting in a low conductivity of 10⁻⁷ S cm⁻¹. Many of the PEO-based SSBs are operated at elevated temperatures to increase the lithium-ion conductivity, which may introduce thermal degradation and thermal safety concerns. PEO presents a low elastic modulus at the 106 Pa level at room temperature. When operated at elevated temperatures, the crystallinity of PEO decreases and the solid electrolyte softens leading to worse mechanical strength to resist lithium dendrite growth. The narrow electrochemical window is another challenge restricting the large-scale application of PEO-based SSBs. A high valent state transition metal in the cathode is reported to catalyse the dehydrogenation and decomposition of PEO chains starting at a low voltage of 3.8 V (vs. Li/Li⁺). The polymer nature of the PEO-based SSEs also brings thermal stability concerns. PEO may thermally decompose at around 150 °C, which is much lower than that of inorganic SSEs.

In this work, we attempt to review the different strategies to optimize the performance of PEO-based SSBs in terms of enhancing lithium-ion mobility, mechanical strength and thermal/electrochemical stability as shown in Fig. 2. Besides, advanced characterization methods to investigate the ion

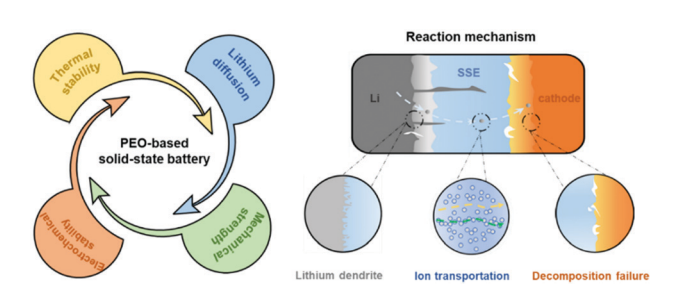


Fig. 2 Main limitations of PEO-based solid-state electrolytes

transportation, lithium dendrite growth and decomposition failure mechanism will also be introduced.

2. Developing high performance PEO-based SSBs

2.1 Lithium-ion diffusion ability

Lithium diffusion across the electrode/electrolyte interface and within the electrolyte dominates the rate performance of SSBs. The ionic conductivity evaluates the lithium diffusion ability within SSEs. PEO presents high lithium ion solubility but poor lithium ion conductivity at room temperature (less than 10⁻⁷ S cm⁻¹). While the lithium-ion mobility occurs through the movement of PEO chain segments and lithium ion "coordination-dissociation" effect, more than 50 wt% of PEO crystallinity at room temperature leads to less freely moveable PEO chains in the amorphous state.17 The strong ionic bond between lithium ions and anions constrains the free movement of lithium ions. As the lithium ions are easily coordinated with the ether units (EO structure) of PEO, it also increases the energy barrier for free Li⁺ migration, leading to a low Li⁺transference number. Thus, more efforts have been devoted to reducing the crystallinity of PEO, increasing the Li+transference number and promoting the anion dissociation to improve the overall ionic conductivity of PEO-based SSEs. On the other hand, the lithium diffusion behaviour at the electrolyte/electrode interface not only affects the lithium dendrite growth owing to non-uniform lithium-ion deposition, but also affects the rate performance dominated by the interfacial charge transfer especially on the cathode side. While many strategies deliver the synergistic effect on reducing crystallinity, promoting the lithium salt dissociation or increasing the Li+ transference number, we attempt to give a brief summary on the typical attempts toward each effect.



ChemComm

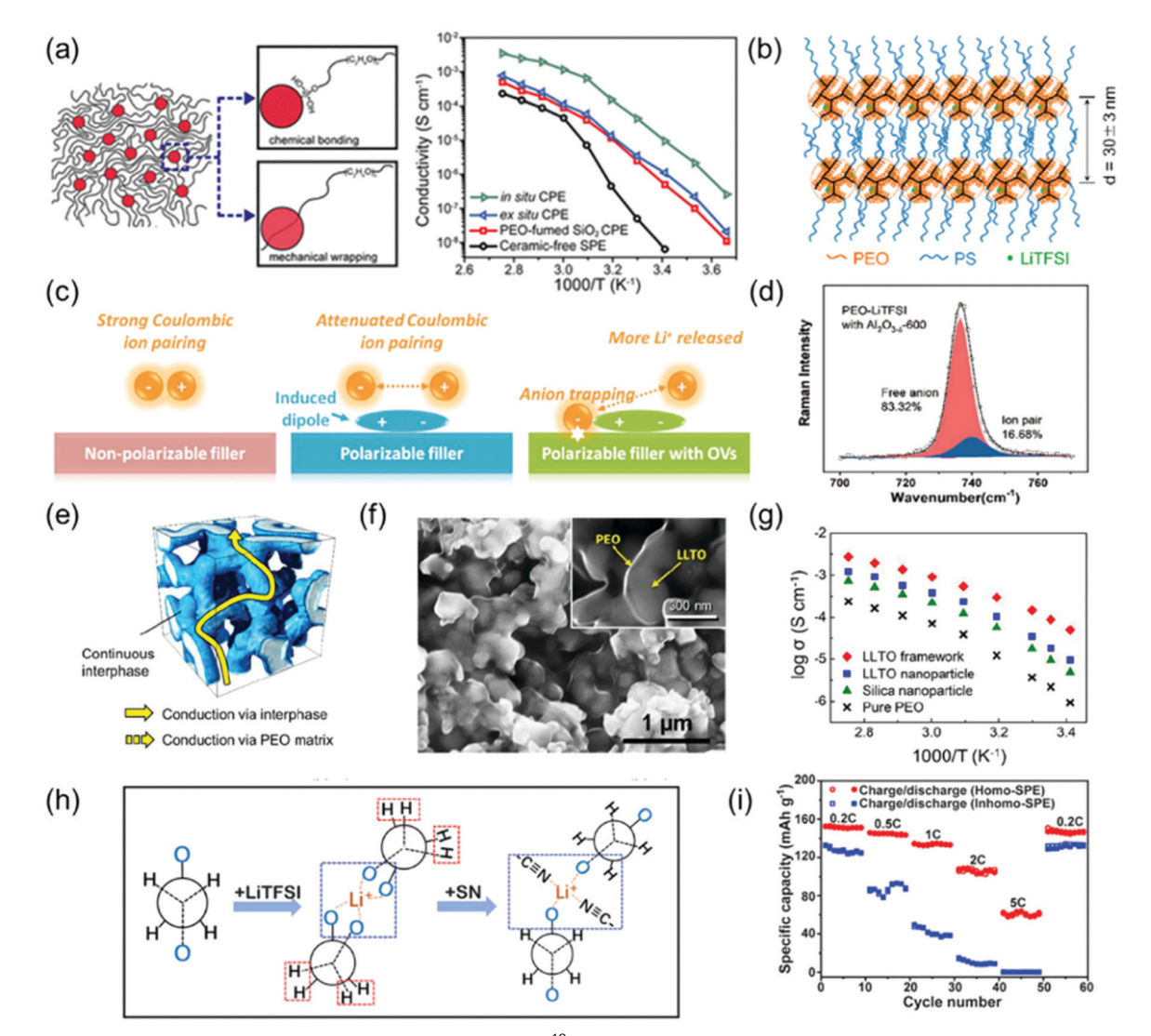


Fig. 3 Improving lithium-ion conductivity. (a) MUSiO₂ as an inert filler. Reproduced with permission. Copyright © 2015 American Chemical Society. (b) Hyperbranched topological structure formed between PS and PEO chains. 19 Reproduced with permission. Copyright © 2019 American Chemical Society. (c) Oxygen vacancy induced polarizable filters and the (d) Raman result of the lithium salt dissociation.²⁰ Reproduced with permission. Copyright © 2021 Wiley-VCH GmbH. (e) 3D LLTO as an active filler for the PEO-based electrolyte, (f) SEM image of the composite electrolyte and (g) ionic conductivity of various electrolytes.²¹ Reproduced with permission. Copyright © 2018 Wiley-VCH Verlag GmbH & Co. (h) SN as a plasticizer and (i) improved rate performance.²² Reproduced with permission. Copyright@2020 Wiley-VCH GmbH.

Reducing crystallinity. Many strategies have been demonstrated to increase the amorphous region and decrease the glass transition temperature (T_g) in the PEO electrolyte, including inorganic fillers, physical mixing, and copolymerization with organic components. The widely reported inorganic fillers include inert fillers and active fillers. The inert fillers including SiO₂, Al₂O₃, ZrO₂, TiO₂, etc. have negligible lithium-ion conductivity, but serve as cross-linking centers to reconstruct the PEO structure by the interfacial interaction between inert fillers and the PEO chains.²³ Cui's group developed monodispersed ultrafine SiO2 (MUSiO2) via in situ hydrolysis of tetraethyl orthosilicate (TEOS) in the PEO solution to modify the PEObased solid-state electrolyte¹⁸ (Fig. 3(a)). A stronger chemical/ mechanical interaction between MUSiO2 and PEO chains was built with hydroxyl groups on MUSiO2 during in situ synthesis,

which pinned PEO chains locally and decreased crystallization leading to even 1 order of magnitude higher lithium ion conductivity than its counterpart by simple mechanical mixing.

Functional polymers are also introduced to bend or crosslink the PEO chains to suppress the PEO crystalline phase. For example, polyacrylonitrile (PAN) with a rich electron polar nitrile (-C≡N) group is reported to have a strong bending effect toward the H atom in PEO.34 More free ion areas can be observed by FTIR spectroscopy, implying an improved ionic conductivity. Yao et al. developed a hyperstar structure polymer electrolyte with the addition of linear polystyrene (PS). 19 The rigid PS served as "arms" to interact with PEO chains to form a hyperbranched topological structure (Fig. 3(b)). Thus, PEO crystallization can be suppressed, and the PEO segmental motion can be tuned by controlling the average chain length

of the branched PEO segments and PS, leading to an improved ionic conductivity of $9.5 \times 10^{-5} \text{ S cm}^{-1}$.

Feature Article

Lithium salt dissociation and Li⁺-transference number. The extra interaction between anions and polymer/fillers should be introduced to release the lithium ion from the ionic pairing and suppress the anion mobility. For example, Lu et al. synthesized a novel hydroxypropyl trimethylammonium bis(trifluoromethane) sulfonimide chitosan salt (HACC-TFSI) by an ion exchange reaction and used it as the lithium salt for PEO-based SSBs.35 Interactions between quaternary ammonium groups and TFSI- anions succeeded in increasing the dissociation of the LiTFSI salt and improving the ionic conductivity. Cui et al. introduced Y2O3-doped ZrO2 nanowires enriched with positive-charged oxygen vacancies as fillers for the PEO-based electrolyte.36 Positively charged oxygen vacancies on the surfaces of fillers created a stronger affinity with ClO₄ revealed by Raman spectroscopy. More free Li ions can be released to deliver higher lithium conductivity and increased lithium transference number. Inspired by their work, Pan et al. also introduced an interfacial oxygen vacancy on the Al₂O₃ filler to promote the dissociation of the lithium salt.20 A tunable concentration of the oxygen vacancy can be introduced on Al₂O₃ particles via thermal reduction with NaBH4. The localized induced dipole is generated when the free charges within polarizable fillers interact with ion pairs (Fig. 3(c)). Thus, fillers loading oxygen vacancy preferentially interact with anions and weaken the coulombic attractions within the ion pairs to dissociate these ions and encourage free Li⁺ (the Raman result is shown in Fig. 3(d)) to move. Various organic anion acceptors have also been introduced to enhance the lithium ion transference number.³⁷ Strong ion-dipole interaction between an anion and an acceptor is created through polar groups such as boron-based, amido-based, or calixarene.³⁷ Li et al. added aramid nanofibers (ANFs) constituted with polyparaphenylene terephthalamide (PPTA) into the PEO electrolyte.³⁸ The abundant amide groups bring the hydrogen-bond interactions between the amide groups of the ANFs and the PEO chains and anions, not only effectively suppressing the PEO crystallization, but also promoting the LiTFSI dissociation. When the anion is immobilized or with negligible mobility by covalent linking, single-ion conductor electrolytes (SICEs) are developed with a high Li⁺-transference number (over 0.8).³⁷ Liu et al. designed a new single lithium-ion conducting lithium poly[(cyano)(4styrenesulfonyl)imide] (LiPCSI) as the substitute for the traditional

LiTFSI salt in the PEO electrolyte. 39 The strong electron-withdrawing cyano groups (-C=N) on LiPCSI significantly promote the anionic delocalization, contributing to a high Li⁺-transference number of 0.84 for the optimized PEO₈-LiPCSI electrolyte.

Embedded additional lithium-ion pathways. Active fillers can affect the crystallinity of polymers by interacting with polymer electrolytes and promote the dissociation of lithium salts by attracting anionic groups. More importantly, active fillers with a lithium-ion conductivity are reported to construct additional embedded conductive networks to facilitate the lithium-ion diffusion. Yu et al. introduced a three dimensional nanostructured hydrogel-derived Li_{0.35}La_{0.55}TiO₃ (LLTO) framework into the PEO electrolyte.21 Benefiting from the additional lithium-ion pathway in the 3D LLTO/PEO electrolyte (Fig. 3(e) and (f)), a high ionic conductivity of $1.5 \times 10^{-4} \text{ S cm}^{-1}$ at 30 °C was achieved (Fig. 3(g)). Various inorganic solid electrolytes have been employed to develop the composite inorganic solid electrolyte/polymer electrolyte as shown in Table 1. By varying the concentration, morphology, and interfacial composition of the active filters, the lithium-ion conductivity can be optimized. D. Rettenwander et al. investigated how the content of LLZO fillers affected the performance of the PEO-based electrolyte. 40 With a higher filler concentration (20 wt%), the crystallinity increased because the excessive LLZO in the electrolyte restrain the segmental motion of the polymer chains and led to a lower ionic conductivity than a lower filler concentration electrolyte (10 wt%). Goodenough et al. investigated the effect of the filler concentration on the lithium ion diffusion and conductivity. 12 The percolation threshold was defined corresponding to the content of LLZTO fillers in PEO-LLZTO composite electrolytes, where an alternative Li⁺ transfer pathway appears. In the "ceramic in the polymer" type composite electrolyte (10 wt% LLZTO content), the lithium ion diffusion mainly occurred in the polymer regions. The lithium ion conductivity was provided both in the polymer and LLZTO regions (intermediate type composite electrolyte, 50 wt% LLZTO). While in the "polymer in ceramic" type composite electrolyte, LLZTO ceramic dominated the lithium ion conductivity.

Plasticizer and nano-wetting. A plasticizer has been introduced into the solid polymer electrolyte to improve the ionic conductivity and mitigate large interfacial resistance. The widely used plasticizer in SPE includes an organic electrolyte,

Table 1 Typical active fillers for the PEO-based electrolyte and the corresponding electrochemical performance

Electrolyte composition	Ionic conductivity	Cycle performance	Ref.
PEO-15 wt% LLTO-LiTFSI	$2.4 imes10^{-4}, 25~^\circ\mathrm{C}$	0.5 mA cm ⁻² , 720 h, 25 °C	24
PEO-26 wt% LAGP-LiTFSI	$1.1 \times 10^{-3}, 60 ^{\circ}\text{C}$	$0.1 + 0.3 \text{ mA cm}^{-2}$, 200 h, 60 °C	25
PEO-70 wt% LATP-LiTFSI	$7.9 \times 10^{-5}, 60 ^{\circ}\text{C}$	0.2 mA cm ⁻² , 180 h, 60 °C	26
PEO-bp-15 wt% LATP-LiTFSI	$3.3 \times 10^{-3}, 30 ^{\circ}\text{C}$	2.0 mA cm ⁻² , 1100 h, 30 °C	27
PEO-10 wt% LLZO-LiTFSI	$2.39 \times 10^{-4}, 25 ^{\circ}\mathrm{C}$	1.0 mA cm ⁻² , 1000 h, 60 °C	28
PEO-50 wt% LLZO-LiTFSI	2.73×10^{-4} , 60 °C	0.1 mA cm ⁻² , 400 h, 60 °C	29
PEO-20.7 wt% LLZAO-LiClO ₄	2.25×10^{-5} , 30 °C	0.3 mA cm ⁻² , 100 h, 60 °C	30
PEO/PEG-60 wt% LLZTO-LiTFSI	$1.17 \times 10^{-4}, 30 {}^{\circ}\mathrm{C}$	0.5 mA cm ⁻² , 670 h, 55 °C	12
PEO-10 wt% LLZTO-LiTFSI	$1.12 \times 10^{-5}, 25 {}^{\circ}\mathrm{C}$	0.2 mA cm ⁻² , 800 h, 60 °C	31
PEO/PEG-3 wt% LGPS-LiTFSI	$9.83 \times 10^{-4}, 25 ^{\circ}\text{C}$	0.5 mA cm ⁻² , 3200 h, 50 °C	17
PEO-1 wt% LSPS-LiTFSI	$1.69 \times 10^{-4}, 50 ^{\circ}\text{C}$	0.1 mA cm ⁻² , 600 h, 60 °C	32
PEO-10 wt% LiAlSiO ₄ -LiTFSI	$4.68 \times 10^{-4}, 60 ^{\circ}\mathrm{C}$	0.1 mA cm ⁻² , 225 h, 60 °C	33

ChemComm

ionic liquid, and organic with a small molecular weight. As a typical plasticizer, succinonitrile (SN) contains cyano groups which can dissociate alkali metal salts into ions through the coordination. 41 Xu et al. prepared a PEO-LiTFSI-1 wt% LGPS-10 wt% SN solid electrolyte (Fig. 3(h)).42 The addition of SN decreased the PEO crystallinity and decreased the T_{σ} to 46.18 °C, leading to an optimized lithium-ion conductivity of $9.10 \times 10^{-5}~\mathrm{S~cm^{-1}}$ at 25 $^{\circ}\mathrm{C}.~\mathrm{Li}$ et al. increased the SN content with a high SN/EO molar ratio (SN: EO = 1:4) and constructed a free-standing solid electrolyte membrane.22 Homogeneous and fast ion transport channels were created with a lower lithium salt concentration (Li⁺: EO = 1:32), delivering a high lithiumion conductivity of 0.19 mS cm⁻¹ 25 °C and much improved rate performance (Fig. 3(i)). Ionic liquid and conventional liquid electrolyte solvents such as Pyr_{A,4}TFSI, 43 DMSO, 44 ethylene carbonate and propylene carbonate⁴⁵ have also been reported as effective plasticizers to increase the ionic conductivity of the PEO-based electrolyte and promote the interfacial lithium diffusion by a nano-wetting effect. However, the liquid flammable plasticizer may sacrifice the safety ability which

Close contact and interfacial lithium ion diffusion. During the repeated lithium ion deposition and stripping process, voids will form on the lithium metal/composite electrolyte surface, leading to elevated interfacial resistance for lithium ion diffusion. Li et al. introduced the methyl 2-hydroxyethyl cellulose as an organic filler into the PEO-based electrolyte. 46 The porous texture in the polymer created the 3D contact interface of lithium metal/electrolyte. The enhanced anode-electrolyte interface compatibility was favourable for stable Li plating/stripping cycling for over 1000 cycles with a low overpotential (75 mV). Pan et al. added boronized polyethylene glycol (BPEG) into the composite PEO electrolyte. 47 Planar BPEG oligomers achieved a "soft contact" on the anode-electrolyte surface to deliver low interfacial polarization. PEO is reported to be reduced on the lithium metal surface to increase the interfacial resistance. Tao et al. demonstrated localized iodization at the anode-electrolyte interface to promote interfacial lithium diffusion.⁴⁸ I₂ was added and reacted with PEO chains, enabling the spontaneous formation of a triiodide ion (I₃⁻). The compact and uniform iodine-containing SEI layer contributed to the elevated rate performance.

2.2 Enhancing mechanical properties

needs further optimization.

Different from conventional organic separators, solid electrolytes not only separate the cathode and anode but also serve as the lithium-ion conductor. Non-uniform lithium deposition under electrochemical/thermal/mechanical abuse conditions increase the possibility of the lithium dendrite growth, which demand for the improved mechanical strength of solid electrolyte separators. PEO possess good flexibility and processability, however low elastic modulus (the Young's modulus of the pure PEO/LiTFSI is about 0.1 MPa⁴⁹). Different strategies have been demonstrated to improve the mechanical strength of the PEO-based solid electrolyte.

Reinforcing and toughening by rigid fillers. It has been widely reported that rigid inorganic fillers can be employed to improve the mechanical strength of the polymer.⁷ The

inorganic fillers can rearrange the stress distribution within the polymer and buffer more deformation energies by yielding polymer chains. 50,51 Inspired by the toughening effect of inorganic fillers toward the polymer, various inorganic fillers with different morphologies/particle sizes/interfacial chemical properties have been introduced to polymer electrolytes to improve mechanical strength. For example, MnO2 nanosheets (Fig. 4(a)) were added to PEO electrolytes by Ding's group. 52 The 5 wt% MnO₂ nanosheets can increase the tensile strength of PEO from 0.56 to 1.27 MPa (Fig. 4(b)). The maximum fracture deformation increases from 858% to 1045%. Profiting from the improved mechanical strength, the lithium symmetrical battery with MnO2 nanosheet modified PEO electrolytes could stably cycle at 0.1 mA cm⁻¹ for over 800 hours at 60 °C without a shortcircuit. Modifying the interface of inorganic fillers with functional groups will further strengthen the interaction between polymer chains and fillers.

Enhancing the molecular interaction by organic fillers. The hydrogen and ether oxygen groups on the PEO chains provide active cross-linking sites for other organic polymers. The enhanced molecular interaction or stronger bonding will help in creating the robust mechanical framework. Li et al. introduced the tetrabutylammonium chloride (TBAC) modified polyvinylidene fluoride (T-PVDF) nanofiber into PEO.53 The staggered T-PVDF nanofibers formed a strong skeleton support in the PEO-based electrolyte owing to the hydrogen bond between PVDF and PEO (Fig. 4(c)). As comparison, the breaking strength of the T-PVDF/PEO electrolyte is improved to 7.8 MPa, about three times larger than the pure PEO. The lithium symmetrical battery with the T-PVDF/PEO composite electrolyte can stably cycle at 0.3 mA cm⁻¹ for more than 1000 hours at 70 °C (Fig. 4(d)). Numerous crosslinked solid polymer electrolytes based on various crosslinking technologies (e.g. ultraviolet (UV) light and thermopolymerization) have been developed such as polyether polymers, acrylate polymers, polyurethane polymers, 56-58 etc. Lee et al. demonstrated simple one-pot polymerization using poly(ethylene glycol) methyl ether methacrylate (PEGMA), a tannic acid (TA)-based crosslinking agent and a plasticizer which can be induced by ultraviolet (UV) light.⁵⁹ The Young's modulus and tensile strength can be elevated to 53.5 MPa and 2.1 MPa, respectively.

While the molecular interaction can be regulated by different functional groups of the introduced polymer, it is possible to synergistically improve the mechanical strength and other electrochemical properties. For example, Pan *et al.* used the polymer of intrinsic microporosity (PIM-1) to improve the mechanical properties of PEO and employed the composite electrolyte for Li–S batteries. The rigid mechanical properties of PIMs (Fig. 4(e)) help in increasing the tensile strength of the PEO-based composite electrolyte from 0.3 MPa to 0.9 MPa, the maximum deformation of over 2000% (Fig. 4(f)), and the modulus of over 8.48 GPa with only the 8 wt% PIM-1 composition (Fig. 4(g)). With the improved mechanical strength and the electrophilic functional groups to trap polysulfide, the asprepared flexible solid-state Li–S batteries show a significantly improved rate, cycling and safety performance.

Feature Article

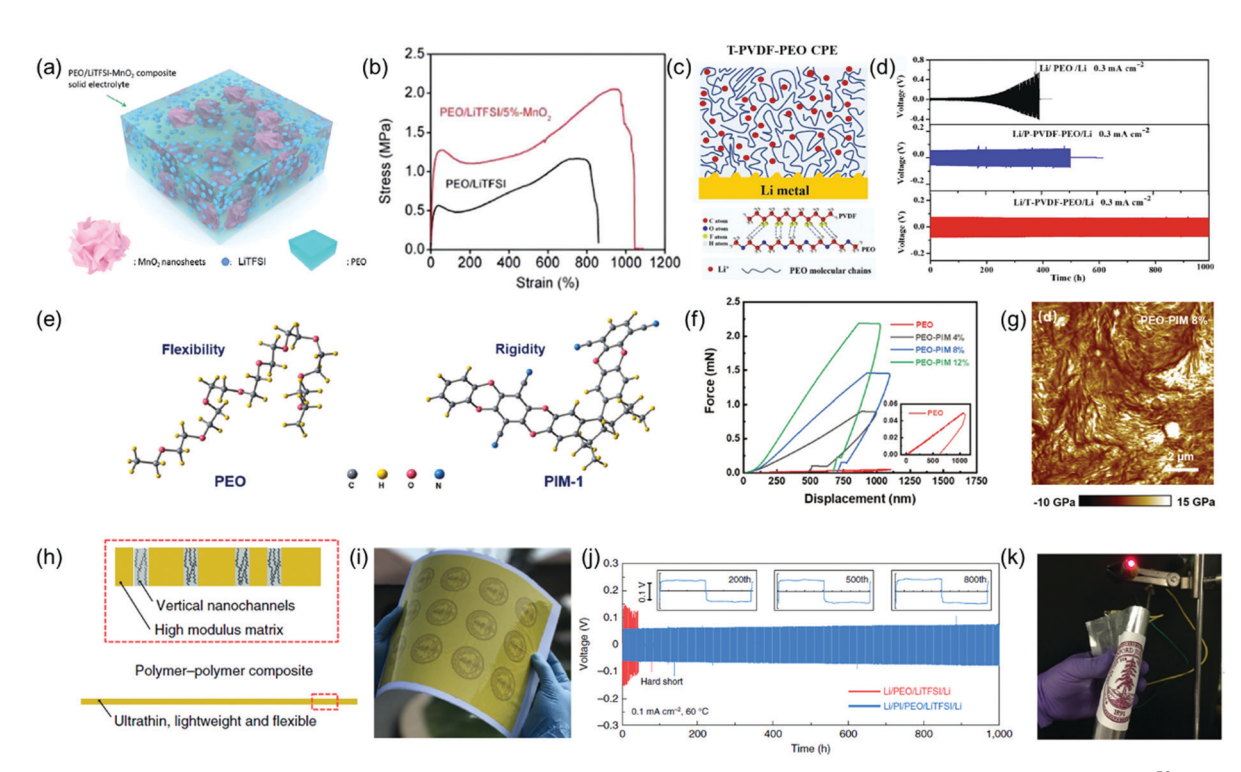


Fig. 4 Enhancing the mechanical stability of PEO-based solid-state electrolytes. (a) Rigid MnO₂ as fillers and (b) stress-strain curves. ⁵² Reprinted with permission. Copyright (i) The Royal Society of Chemistry 2020. (c) Interactions between T-PVDF and PEO and (d) voltage profiles of the Li/Li symmetric batteries. 53 Reproduced with permission. Copyright © 2020 Elsevier B.V. (e) Molecular structures and properties of PEO and PIM-1, (f) load-displacement curves and (g) PEO-PIM modulus distribution. 54 Reproduced with permission. Copyright © 2021 Wiley-VCH GmbH. (h) PI film as the supporting framework, (i) large-scale porous PI film, (j) long-term cycling of symmetrical Li–Li cells and (k) flexible pouch cell based on the optimized electrolyte. 55 Reproduced with permission. Copyright © 2019, The Author(s), under exclusive licence to Springer Nature Limited.

Robust supporting framework. As the intrinsic mechanical strength of PEO is limited, introducing a robust framework as the PEO host can also improve the mechanical properties of the PEObased composite electrolyte. Cui et al. filled the PEO electrolyte into nano-porous polyimide (PI, as shown in Fig. 4(h) and (i)) hosts to develop an ultra-thin solid membrane with a 8.6 micro-meter in thickness.⁵⁵ Benefiting from the remarkable improved mechanical strength (the maximum tensile strength increased by about 400 times), the lithium symmetrical battery with PEO-PI could be stably operated over 1000 hours without a short-circuit (Fig. 4(j)) and flexible pouch cells can be operated under abuse mechanical conditions (Fig. 4(k)). Besides the above commercial porous membrane, other methods such as free-drying, electrospinning, 3D printing, etc. have also been introduced to create a robust mechanical framework as the PEO supporting host. Luo et al. prepared an ultrathin and porous ceramic vermiculite film by electrospinning and with a fused PEO electrolyte. 60 The thin solid electrolyte with a 4.2 um thickness provided an elastic modulus of 175 GPa, contributing to stable cycling under 1 mA cm⁻² at a high capacity of 4 mA h cm⁻².

2.3 Improving electrochemical stability window

PEO-based SSBs are often matched with the LiFePO₄ cathode because of its limited electrochemical stability window (below 4.0 V). The PEO electrolytes undergo severe decomposition when matched with high voltage cathodes (such as $LiNi_xCo_yMn_{1-x-y}O_2$ and $LiCoO_2$). 61,62 Improving the electrochemical stability window of PEO and slowing down the decomposition rate of PEO at high voltage have become the one of the key problems for the industrialization of PEO.

Molecular design and intrinsic stability. Adjusting the molecular structure of the polymer can change the frontier orbital energy level and improve the intrinsic electrochemical stability. Sun et al. studied the effect of the terminal group (-OH and -OCH₃, molecular structure shows in Fig. 5(a)) on the electrochemical properties of polyether solid electrolytes. 63 The terminal group -OH in PEO-based SSEs is the major limiting factor for the narrow electrochemical stability window. When replacing -OH with the -OCH₃ terminal group, the electrochemical stability window can be expanded to 4.3 V (Fig. 5(b)). The assembled Li-LiNi_{0.5}Co_{0.3}Mn_{0.2}O₂ (NCM532) deliver a stable cycling performance (2.0-4.3 V, 0.47 mA h cm⁻², 90% capacity retention after 110 cycles, as shown in Fig. 5(c)).

Functional fillers. While the intrinsic electrochemical stability of PEO is limited, introducing functional fillers with high stability to buffer the decomposition driving force has been regarded as an efficient strategy to improve the electrochemical stability window of the composite PEO electrolyte. Xu et al. introduced a novel cationic metal-organic framework (CMOF) as the filler into the PEO electrolyte. 64 The -NH2 group on the CMOF interacts with the ether oxygen of PEO chains by hydrogen bonds (Fig. 5(d)), leading to an expanded electrochemical

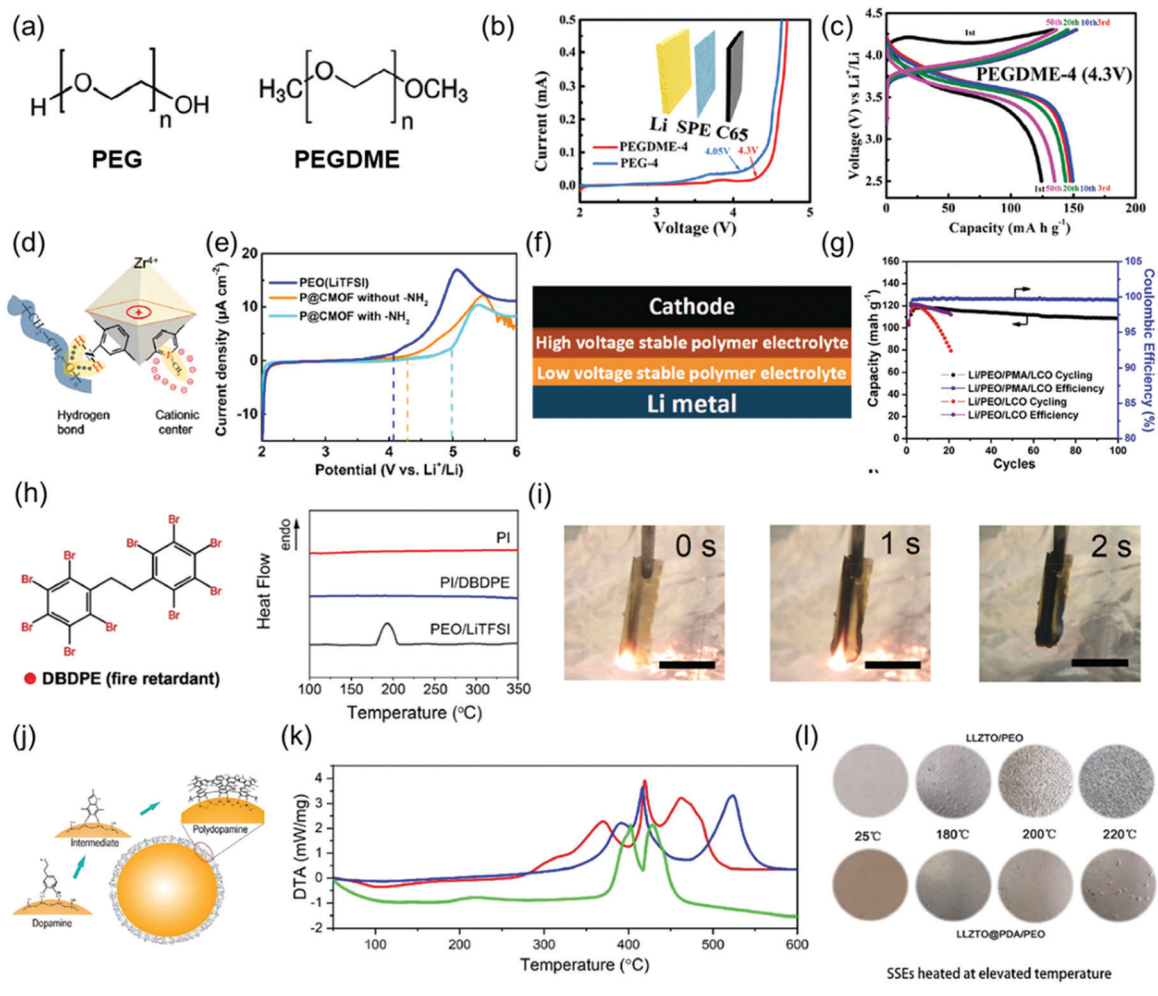


Fig. 5 Electrochemical stability and thermal stability. (a) Molecular structures of PEG and PEGDME, (b) elevated electrochemical window and (c) cycling performance Li-NMC532 coin cells using PEGDME (PEG)-4 SPEs with operating voltage ranges of 2.5–4.3 V.⁶³ Reproduced with permission. Copyright© The Royal Society of Chemistry 2020. (d) Interactions between PEO chains and CMOF and (e) improved electrochemical stability.⁶⁴ Reproduced with permission. Copyright©2019 Published by Elsevier B.V. (f) Stacking model of the double layer electrolyte and (g) cycle performance of solid-state LiCoO₂ batteries.⁷⁰ Reproduced with permission. Copyright©2018 WILEY-VCH Verlag GmbH & Co. (h) Molecular structure of DBDPE and the DSC result of different electrolytes, (i) flame test.⁴⁹ Reproduced with permission. Copyright©2020 American Chemical Society. (j) PDA coated LLZTO, (k) DSC result and (l) images of the solid-state electrolytes when heated at elevated temperature.⁷⁹ Reproduced with permission. Copyright© The Royal Society of Chemistry 2019.

stability window of 4.97 V (Fig. 5(e)) and stable cycling performance with high-voltage LiFe $_{0.15}$ Mn $_{0.85}$ PO $_4$. *In situ* polymerized polydopamine (PDA) nanoparticles were used as fillers for the PEO-based solid electrolyte by Wang's group. ⁶⁵ The large amount of polar groups on the PDA could form H-bonds with ether groups on PEO chains. The enhanced molecular interaction extended the electrochemical stability window to 4.6 V. Other fillers with high electrochemical stability such as graphene, ⁶⁶ various MOFs, ⁶⁷ porous polyamine, ⁶⁸ and polydopamine coated TiO₂ nanofibers ⁶⁹ can also improve the electrochemical window and match with the high-voltage cathode.

Introducing the protective interlayer. Transition metals with high valent state and catalytic activity will aggravate the PEO decomposition. Preventing the direct contact between PEO and positive electrodes by the protective interlayer can also effectively alleviate the oxidation of PEO. Goodenough *et al.*

designed a double-layer solid electrolyte (double-layer PEO-PMA, as shown in Fig. 5(f)) to match with the LiCoO₂ cathode.⁷⁰ Poly(N-methyl-malonic amide) (PMA), as a widely used electrolyte additive or a coating layer to prevent the electrolyte decomposition at high voltage, was mixed with LiTFSI and contacted with the LiCoO₂ electrode. The high electrochemical stability of PMA elevated the electrochemical stability window up to 4.75 V ensuring the stable cycling of the 4 V LiCoO₂ battery over 100 cycles (Fig. 5(g)). Coating the cathode material to avoid direct contact with PEO is also effective to improve the high-voltage performance of PEObased SSBs. Li et al. coated the LiCoO2 (LCO) cathode with the Li_{1.4}Al_{0.4}Ti_{1.6}(PO₄)₃ (LATP) solid electrolyte. 62 LATP with high stability toward the high voltage cathode could effectively mitigate the PEO decomposition catalysed by the LCO interface and increase the electrochemical stability window up to 4.5 V.

Feature Article ChemComm

Other coating layers such as lithium niobium oxide, 71 lithium tantalate, 72 Li₃PO₄, 73 organic layers, 74 etc. are also effective to isolate cathode particles and mitigate the decomposition of the PEO-based electrolyte.

In situ formed protective layers during battery cycling could also protect the PEO from oxidation at high potential. The lithium salt, additives or functional groups on the polymer chains will decompose at high voltage to form a stable interface (similar to artificial CEI in conventional lithium-ion batteries^{75,76}) coated on the cathode. Chen et al. in situ electro-deposited a PAN-based coating layer on the whole cathode (NCM532) interface using a precursor solution (1 M LiDFOB and 10 wt% AN in ethylene carbonate/dimethyl carbonate (EC/DMC)). LiDFOB and the AN additive will decompose to form a stable organic interface to provide an elevated electrochemical stability window of 4.8 V and enable the stable cycling of PEO-based SSBs over 200 cycles. Electrolyte additives are able to widen the electrochemical window of the liquid electrolyte as a sacrificial agent via pre-oxidation.⁷⁷ Li et al. introduced LiPO₂F₂ as the additive for the PEO-based electrolyte.⁷⁸ LiPO₂F₂ will decompose at 4.0 V before PEO (4.8 V). The improved electrochemical stability ensured the stable cycling of LCO|-PEO-LiPO₂F₂-LiFSI|Li batteries for over 100 cycles.

2.4 Improving thermal stability

Conventional lithium batteries are often involved in some thermal related hazards such as smoke, fire, or explosion because of the limited thermal stability of the organic electrolyte, especially under electrochemical/mechanical/thermal abuse conditions. Thermal safety concerns are still associated with the PEO polymer owing to its organic flammable nature. PEO is reported to soften at around 65 °C and decompose over 150 °C accompanied by the formation of small molecule degradation products and gas release.80 While the PEO-based SSBs are often tested at elevated temperature, improving the thermal stability of the PEO electrolyte is essential for the safe operation in practical situations. In principle, fire-proof or thermal stable components should be introduced in the PEObased composite electrolyte to enhance the thermal stability. In the previous section, strategies to strengthen the mechanical stability of PEO-based SSBs have been introduced, many of which could also enable high temperature operation of PEObased solid electrolytes. More examples specifically aimed to improve the thermal stability of the PEO-based electrolyte are introduced in this section.

Various organic or inorganic fire-proof agents have been introduced to improve the thermal stability of the PEO-based electrolyte. Cui et al. added a fire-retardant additive (decabromodiphenyl ethane, DBDPE, as shown in Fig. 5(h)) into the PEO electrolyte. 49 DBDPE will degrade to generate bromo free radicals (Br•) at high temperature and further react with the highly reactive radicals H* and OH* emitted by the burning electrolyte. The heat transfer and release will be limited by the formation of gas products (H2O, Br2 and HBr). Consequently, the DBDPE modified solid state batteries exhibit high tolerance to thermal abuses such as flame tests (Fig. 5(i)). While the halogen product might be harmful to the environment, Hu et al. introduced aluminum diethyl hypophosphite (ADP) into the PEO electrolyte.81 ADP as a halogen-free and environmentally friendly flame retardant enables the self-extinguish ability by forming hypophosphite and other substances to prevent the combustion of PEO electrolytes.

Inorganic fillers with non-flammable properties can also improve the high temperature tolerance of PEO-based SSBs. Hexagonal boron nitride (h-BN) has an extremely high temperature resistance and is widely used as a refractory material. Min et al. added h-BN nanosheets as fillers into the PEO-based electrolyte (PLSB).82 The decomposition temperature of the h-BN and SiO2 modified solid electrolyte was elevated to around 450 °C (much higher than that of the PEO/LiTFSI, around 366 °C). When exposed at 150 °C, the commercial Celgard 2300 membrane contracted quickly while the as-prepared PLSB membrane maintained its original structure. Benefiting from the improved thermal stability, the as-prepared solid LFP batteries can be stably and safely cycled at 2 C under 150 °C for over 1000 cycles. Wang et al. added polydopamine (PDA) modified Li_{6.4}La₃Zr_{1.4}Ta_{0.6}O₁₂ (LLZTO) nanoparticles (Fig. 5(j)) into the PEO electrolyte.⁷⁹ The thermal decomposition temperature can be significantly increased from around 200 °C to 350 °C (Fig. 5(k)) and the PDA-coated LLZTO/PEO solid-state electrolytes were stable even when heated at elevated temperature (Fig. 5(1)).

Characterization

The practical application of solid polymer batteries often shows low capacity, poor cycle stability and fast degradation due to sluggish lithium-ion diffusion, uncontrollable lithium dendrite growth and electrochemical/thermal/mechanical instability.8 A comprehensive understanding of lithium-ion transportation/ deposition and the interfacial side reaction is essential for the improvement of solid polymer batteries. In this section, advanced characterization methods toward the ion transportation mechanism, lithium dendrite growth and interfacial decomposition are discussed (shown in Fig. 6).

3.1 Ion transportation mechanism

Traditional electrochemical techniques including EIS, CV, etc. have been widely used to investigate the lithium-ion diffusion in SSBs. The impedance spectrum obtained by EIS testing can be used to calculate the lithium-ion conductivity and Li⁺transference number.20 XRD, DSC, and TGA are often used to investigate the crystallinity related to the lithium-ion conductivity of polymer electrolytes. 49 Solid nuclear magnetic resonance (NMR) is a powerful tool to reveal the local structure environment and investigate the lithium-ion dynamics.83 Hu et al. detected the lithium-ion diffusion path in PEO-LLZO composite solid electrolytes by isotope labelling (⁶Li → ⁷Li replacement) assisted solid-state NMR techniques.84 The NMR relaxation time is measured in composite solid electrolytes with different amounts of LLZO, where the lithium-ion enrichment

ChemComm Feature Article

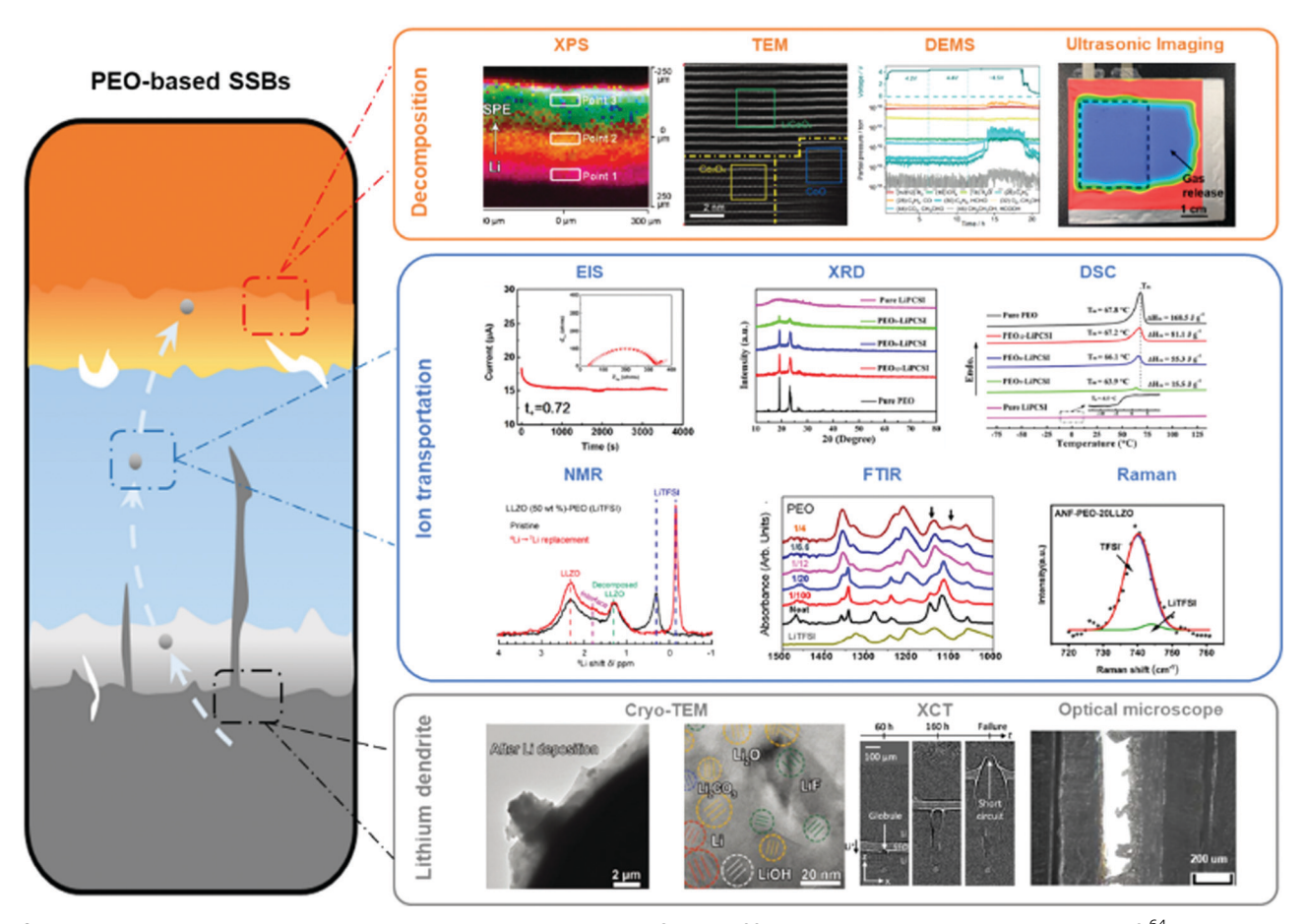


Fig. 6 Advanced characterization methods and reaction mechanism in PEO-based SSBs. Ion transportation characterization: EIS, 64 reproduced with permission. Copyright © 2019 Published by Elsevier B.V. XRD and DSC, 39 reproduced with permission. Copyright © 2020, American Chemical Society. NMR spectroscopy,⁸⁴ reproduced with permission. Copyright©2018 American Chemical Society. FTIR spectroscopy,⁸⁵ reproduced with permission. Copyright©2021 American Chemical Society. Raman spectroscopy, 86 reproduced with permission. Copyright©2021 Elsevier B.V. Lithium dendrite growth characterization: cryo-TEM,⁸⁸ reproduced with permission. Copyright © 2020 WILEY-VCH Verlag GmbH & Co. XCT,⁸⁹ reproduced with permission. Copyright©2021 American Chemical Society. Optical microscopy, ⁹⁰ reproduced with permission. Copyright©2019 Wiley-VCH Verlag GmbH & Co. Decomposition failure related compositional characterization: XPS, ⁸⁸ reproduced with permission. Copyright©2020 WILEY-VCH Verlag GmbH & Co. TEM,91 reproduced with permission. Copyright ©2020 WILEY-VCH Verlag GmbH & Co. DEMS,62 reproduced with permission. Copyright@2020 American Chemical Society. Ultrasonic imaging, 92 reproduced with permission. Copyright@2022 American Chemical Society.

shows an obvious difference. Increasing the LLZO content will change the ion transportation pathway from the PEO phase to loosely connected LLZO particles, leading to a lower lithiumion mobility.

Vibrational spectroscopy methods such as FTIR and Raman spectroscopies have been employed to reveal the ion-polymer/ ion-anion interaction by observing the molecular environment. Nealey et al. applied FTIR spectroscopy to investigate ionic solvation and transport behavior in the PEO-based electrolyte. 85 The free and complexed lithium ions with ethylene oxide moieties in the PEO can be identified with different ether peaks. Thus, the lithium-ion solvation in the PEO chains at different lithium salt concentrations can be measured. Raman spectroscopy is also highly sensitive to the conformational change of the lithium salt in the polymer electrolyte. Gao et al. investigated the anion (TFSI⁻) vibration of the PEO-based electrolyte with the Raman spectrum.86 The relative quantity of free TFSI (lithium salt association) and ion pair (solvated

LiTFSI) can be obtained after Raman peak fitting and semiquantitative estimation. The free TFSI proportion in the prepared PEO-ANF-20LLZO electrolyte is as high as 96.3%, leading to the highest Li⁺-transference number and lithium conductivity.

3.2 Growth of lithium dendrites

The critical current density (CCD) has been defined as the highest current density when the lithium metal battery can be stably cycled without drastic lithium dendrite growth and short-circuit. Constant current cycling at various current densities and the corresponding voltage curves are the extensively used electrochemical methods to evaluate the lithium dendrite growth. Besides the traditional electrochemical measurement, multi-scale advanced visual characterization methods should also be introduced to reveal the lithium dendrite growth mechanism.

Feature Article ChemComm

Atomic level. Cryo-transmission electron microscopy (cryo-TEM) has recently received considerable attention due to its ability to observe an organic structure without damages, one of the successful examples is the analysis of the SEI structure and component.87 Tao et al. employed cryo-TEM to observe the atomic structure of the interface between PEO and lithium metal.88 A mosaic interface composed of Li, Li₂O, LiOH, Li₂CO₃ and amorphous polymer region can be observed which will thicken during cycling and lead to short circuit. The addition of Li₂S into the PEO electrolyte can promote the formation of the LiF-rich interface as observed by cryo-TEM, which can prevent not only the side reaction between Li and PEO but also lithium dendrite growth.

Electrode level. Uneven lithium-ion deposition will trigger the formation of initial lithium dendrite nucleation. Continuous dendrite formation will further lead to the penetration into the polymer electrolyte with the final result of membrane destruction and short-circuit. It is also important to directly observe the lithium dendrite growth within the polymer electrolyte. Goodenough et al. used non-destructive synchrotron radiation X-ray tomography to characterize the interface morphology of lithium symmetrical batteries after cycling.⁹³ The Mg(ClO₄)₂-doped PEO electrolyte contributed to a uniform contact with lithium metal and no lithium dendrite nucleation was observed. As a comparison, a mossy lithium morphology with voids was observed in the pure PEO electrolyte. Dendrites gradually penetrated through the pure PEO electrolyte as shown in the reconstructed XCT images.

Cell level. Macroscopical analysis by optical microscopy provides direct visualization of the lithium dendrite growth process.⁹⁴ Wiemhöfer et al. used an optical microscope to directly observe the growth of lithium dendrites in PEO.90 The surface of lithium metal was flat and in good contact with PEO before cycling. After 14 hours of polarization, lithium dendrite formed with a needle-like structure. The continuous formation of lithium dendrite even reached the positive electrode surface after being cycled for 50 hours.

3.3 Decomposition failure

PEO with the limited electrochemical stability is reported to decompose both on the anode and cathode surfaces. On the cathode side, the interface problem is mainly due to the selfdecomposition of PEO at high potential and the reaction with a highly catalytic cathode surface. Meanwhile, on the anode side, the PEO turns to be reduced by the lithium metal. The decomposition reaction usually leads to the formation of the interlayer with side products and further trigger capacity degradation or lithium dendrite growth, which will be aggravated at elevated temperature and even lead to thermal runaway. As the decomposition reaction may involve multiphysical/chemical evolution, advanced characterization methods reveal the chemical information that will be introduced in this section.

Tao et al. employed in-depth XPS to investigate the componential distribution of PEO and the lithium metal interface.88 The introduction of Li₂S into the PEO electrolyte will accelerate

the decomposition of N(CF₃SO₂)₂ contributing to the formation of the LiF-rich interlayer between the lithium metal and PEO. The LiF-rich interface could protect the PEO from being reduced by the lithium metal via inhibiting the breakage of C-O bonds in the PEO electrolyte. On the cathode side, the side reaction can damage both the PEO electrolyte and the cathode electrode. Li et al. investigated the interaction between PEO and LiCoO₂ by soft X-ray absorption spectroscopy (XAS), TEM and XPS. 91 The XAS result shows the partial charge compensation on the ligand oxygen which means that oxygen anions will be oxidized and remained transition metal possess highly catalytic to decompose the PEO electrolyte. Thick Co₃O₄ and CoO were observed on the LiCoO2 surface by highresolution TEM.

Gas release can be also triggered during PEO decomposition. Li et al. employed differential electrochemical mass spectrometry (DEMS) to investigate the gas evolution in PEObased SSBs. 62 When charged to 4.5 V, complex gases were observed including H2, CH4, H2O, C2H2, C2H4, CO, C2H6, HCHO, O2, CH3OH, CO2, CH3CHO, CH3CH2OH, and HCOOH. These highly flammable gases may lead to potential safety issues of SSBs. At the onset voltage of 4.2 V, H2 was detected as the main gas release. The DFT simulation suggested that the decomposition of the PEO electrolyte started with an electron being removed from the oxygen and hydrogen jointly under the catalytic sites of charged state Li_xCoO₂. The continuous and massive gas release will further trigger safety hazards. Li et al. compared the thermal stability of different cathodes (Li₂CoO₂ and Li₂Ni_xMn_yCo₂O₂) against the PEO electrolyte by ARC, Raman spectroscopy and other structural analyses. 95 A passivation layer can be found on the Li₂CoO₂ and PEO interfaces by Raman spectroscopy which can suppress the oxygen release and contribute to a reduced heat generation rate and lower the risk of thermal runaway than Li₂Ni_xMn_yCo₂O₂ and the liquid electrolyte. Huang et al. introduced ultrasonic imaging techniques to study the gas release and interfacial instability in PEObased SSEs.92 Ultrasound attenuates significantly when it passes through gases or voids. When the lithium metal is in contact with the PEO/LLZTO composite electrolyte, the transmitted ultrasonic signal went through significant attenuation indicating the gas existence. With the continuous gas generation, the interfacial resistance doubled only after 1 hour of cycling.

4. Conclusions

In this review, various strategies for improving the comprehensive performance of PEO-based solid-state batteries have been summarized in terms of lithium diffusion ability, mechanical stability, electrochemical stability and thermal stability. With great potential to replace the conventional liquid electrolyte, the PEO-based solid-state electrolyte can be further developed in the following prospected ways:

(1) Practical ionic conductivity at lower temperature. PEObased solid-state batteries are often operated at elevated ChemComm Feature Article

temperature which will increase the safety concerns and operation cost. More efforts should be devoted to decreasing the operation temperature of the PEO-based electrolyte. For example, optimizing the active filler component in composite electrolytes.

- (2) Thin but robust mechanical strength. As many of the reported PEO-based solid electrolyte membranes are thicker than the commercial separator (celgard, etc.), which will sacrifice the energy density, advanced synthesis and processing techniques should be developed to prepare thin PEO-based electrolyte membranes.
- (3) High energy density consideration. Composite PEO electrolytes are often reported to match LiFePO4 in terms of performance. Driven by the continuous increasing demand for high energy density battery systems, more attention should be paid to developing PEO composite electrolytes matching high voltage cathodes (high-nickel, Li-rich cathode, etc.) or Li-S batteries. Meanwhile, the areal mass loading of the active material is still not compatible for many of the reported PEObased solid-state batteries, and advanced electrode preparation techniques should be developed to elevate the areal mass loading while retain sufficient electronic and ionic conductivity.
- (4) Operando and in situ analysis, reliability and feasibility testing techniques at different scales. In-depth investigations toward material interaction and interfacial reactions should be paid more attention to provide more fundamental information. Non-destructive techniques and sensors should be introduced to monitor the operando battery cycling. Safety and reliability testing of the commercial liquid lithium-ion batteries should be performed for their performance evaluation.

Conflicts of interest

There are no conflicts to declare.

Acknowledgements

This work is funded by the National Key R&D Program of China (2021YFB2400200).

Notes and references

- 1 J. Xiang, L. Yang, L. Yuan, K. Yuan, Y. Zhang, Y. Huang, J. Lin, F. Pan and Y. Huang, Joule, 2019, 3, 2334-2363.
- 2 Q. Y. Wang, B. Liu, Y. H. Shen, J. K. Wu, Z. Q. Zhao, C. Zhong and W. B. Hu, Adv. Sci., 2021, 8.
- 3 M.-C. Pang, K. Yang, R. Brugge, T. Zhang, X. Liu, F. Pan, S. Yang, A. Aguadero, B. Wu, M. Marinescu, H. Wang and G. J. Offer, Mater. Today, 2021, 49, 145-183.
- 4 X. Feng, H. Fang, N. Wu, P. Liu, P. Jena, J. Nanda and D. Mitlin, Joule, 2022, 6, 543-587.
- 5 A. Manthiram, X. Yu and S. Wang, Nat. Rev. Mater., 2017, 2, 16103.
- 6 Q. Zhao, S. Stalin, C.-Z. Zhao and L. A. Archer, Nat. Rev. Mater., 2020, 5, 229-252.
- 7 L.-Z. Fan, H. He and C.-W. Nan, Nat. Rev. Mater., 2021, 6, 1003-1019.
- 8 Y. Zheng, Y. Z. Yao, J. H. Ou, M. Li, D. Luo, H. Z. Dou, Z. Q. Li, K. Amine, A. P. Yu and Z. W. Chen, Chem. Soc. Rev., 2020, 49, 8790-8839.

- 9 Y. Jiang, X. Yan, Z. Ma, P. Mei, W. Xiao, Q. You and Y. Zhang, Polymers, 2018, 10, 1237.
- 10 J. Zheng, M. Tang and Y.-Y. Hu, Angew. Chem., Int. Ed., 2016, 55, 12538-12542.
- 11 H. Zhai, P. Xu, M. Ning, Q. Cheng, J. Mandal and Y. Yang, Nano Lett., 2017, 17, 3182-3187.
- 12 L. Chen, Y. Li, S.-P. Li, L.-Z. Fan, C.-W. Nan and J. B. Goodenough, Nano Energy, 2018, 46, 176-184.
- 13 J.-Y. Liang, X.-X. Zeng, X.-D. Zhang, T.-T. Zuo, M. Yan, Y.-X. Yin, J.-L. Shi, X.-W. Wu, Y.-G. Guo and L.-J. Wan, J. Am. Chem. Soc., 2019, 141, 9165-9169.
- 14 O. Sheng, J. Zheng, Z. Ju, C. Jin, Y. Wang, M. Chen, J. Nai, T. Liu, W. Zhang, Y. Liu and X. Tao, Adv. Mater., 2020, 32, 2000223.
- 15 P. Zhang, W. Guo, Z. H. Guo, Y. Ma, L. Gao, Z. Cong, X. J. Zhao, L. Qiao, X. Pu and Z. L. Wang, Adv. Mater., 2021, 33, 2101396.
- 16 L. Zhang, P. Zhang, C. Chang, W. Guo, Z. H. Guo and X. Pu, ACS Appl. Mater. Interfaces, 2021, 13, 46794-46802.
- 17 K. Pan, L. Zhang, W. Qian, X. Wu, K. Dong, H. Zhang and S. Zhang, Adv. Mater., 2020, 32, 2000399.
- 18 D. Lin, W. Liu, Y. Liu, H. R. Lee, P.-C. Hsu, K. Liu and Y. Cui, Nano Lett., 2016, 16, 459-465.
- 19 Y. Chen, Y. Shi, Y. Liang, H. Dong, F. Hao, A. Wang, Y. Zhu, X. Cui and Y. Yao, ACS Appl. Energy Mater., 2019, 2, 1608-1615.
- 20 Y. Song, L. Yang, J. Li, M. Zhang, Y. Wang, S. Li, S. Chen, K. Yang, K. Xu and F. Pan, Small, 2021, 17, 2102039.
- 21 J. Bae, Y. T. Li, J. Zhang, X. Y. Zhou, F. Zhao, Y. Shi, J. B. Goodenough and G. H. Yu, Angew. Chem., Int. Ed., 2018, 57, 2096-2100.
- 22 S. Xu, Z. Sun, C. Sun, F. Li, K. Chen, Z. Zhang, G. Hou, H.-M. Cheng and F. Li, Adv. Funct. Mater., 2020, 30, 2007172.
- 23 Y. Zheng, Y. Yao, J. Ou, M. Li, D. Luo, H. Dou, Z. Li, K. Amine, A. Yu and Z. Chen, Chem. Soc. Rev., 2020, 49, 8790-8839.
- 24 P. Zhu, C. Yan, M. Dirican, J. Zhu, J. Zang, R. K. Selvan, C.-C. Chung, H. Jia, Y. Li, Y. Kiyak, N. Wu and X. Zhang, J. Mater. Chem. A, 2018, 6, 4279-4285.
- 25 X. Wang, H. Zhai, B. Qie, Q. Cheng, A. Li, J. Borovilas, B. Xu, C. Shi, T. Jin, X. Liao, Y. Li, X. He, S. Du, Y. Fu, M. Dontigny, K. Zaghib and Y. Yang, Nano Energy, 2019, 60, 205-212.
- 26 L. Yang, Z. Wang, Y. Feng, R. Tan, Y. Zuo, R. Gao, Y. Zhao, L. Han, Z. Wang and F. Pan, Adv. Energy Mater., 2017, 7, 1701437.
- 27 S. H. Siyal, M. Li, H. Li, J.-L. Lan, Y. Yu and X. Yang, Appl. Surf. Sci., 2019, 494, 1119-1126.
- 28 Z. Wan, D. Lei, W. Yang, C. Liu, K. Shi, X. Hao, L. Shen, W. Lv, B. Li, Q.-H. Yang, F. Kang and Y.-B. He, Adv. Funct. Mater., 2019, 29, 1805301.
- 29 S. Wang, Q. Sun, W. Peng, Y. Ma, Y. Zhou, D. Song, H. Zhang, X. Shi, C. Li and L. Zhang, J. Energy Chem., 2021, 58, 85-93.
- 30 X. Fu, Y. Li, C. Liao, W. Gong, M. Yang, R. K. Y. Li, S. C. Tjong and Z. Lu, Compos. Sci. Technol., 2019, 184, 107863.
- 31 C.-Z. Zhao, X.-Q. Zhang, X.-B. Cheng, R. Zhang, R. Xu, P.-Y. Chen, H.-J. Peng, J.-Q. Huang and Q. Zhang, Proc. Natl. Acad. Sci. U. S. A., 2017, 114, 11069-11074.
- 32 X. Li, D. Wang, H. Wang, H. Yan, Z. Gong and Y. Yang, ACS Appl. Mater. Interfaces, 2019, 11, 22745-22753.
- 33 Y. Wu, X. Li, G. Yan, Z. Wang, H. Guo, Y. Ke, L. Wu, H. Fu and J. Wang, J. Energy Chem., 2021, 53, 116-123.
- 34 A. Arya and A. L. Sharma, J. Mater. Sci.: Mater. Electron., 2018, 29, 17903-17920.
- 35 J. Tan, X. Ao, A. Dai, Y. Yuan, H. Zhuo, H. Lu, L. Zhuang, Y. Ke, C. Su, X. Peng, B. Tian and J. Lu, Energy Storage Mater., 2020, 33, 173-180.
- 36 W. Liu, D. Lin, J. Sun, G. Zhou and Y. Cui, ACS Nano, 2016, 10, 11407-11413.
- 37 Q. Zhou, J. Ma, S. Dong, X. Li and G. Cui, Adv. Mater., 2019, 31, 1902029.
- 38 L. Liu, J. Lyu, J. Mo, H. Yan, L. Xu, P. Peng, J. Li, B. Jiang, L. Chu and M. Li, Nano Energy, 2020, 69, 104398.
- 39 H. Yuan, J. Luan, Z. Yang, J. Zhang, Y. Wu, Z. Lu and H. Liu, ACS Appl. Mater. Interfaces, 2020, 12, 7249-7256.
- 40 M. M. U. Din, M. Häusler, S. M. Fischer, K. Ratzenböck, F. F. Chamasemani, I. Hanghofer, V. Henninge, R. Brunner, C. Slugovc and D. Rettenwander, Front. Energy Res., 2021, 9.
- Y. Ugata, M. L. Thomas, T. Mandai, K. Ueno, K. Dokko and M. Watanabe, Phys. Chem. Chem. Phys., 2019, 21, 9759-9768.
- 42 B. Chen, Z. Huang, X. Chen, Y. Zhao, Q. Xu, P. Long, S. Chen and X. Xu, Electrochim. Acta, 2016, 210, 905-914.

Feature Article ChemComm

- 43 M. Wetjen, M. A. Navarra, S. Panero, S. Passerini, B. Scrosati and J. Hassoun, *ChemSusChem*, 2013, **6**, 1037–1043.
- 44 B. W. Zewde, L. Carbone, S. Greenbaum and J. Hassoun, Solid State Ionics, 2018, 317, 97–102.
- 45 S. N. Banitaba, D. Semnani, E. Heydari-Soureshjani, B. Rezaei and A. A. Ensafi, *Solid State Ionics*, 2020, 347, 115252.
- 46 H. Wu, J. Wang, Y. Zhao, X. Zhang, L. Xu, H. Liu, Y. Cui, Y. Cui and C. Li, Sustainable Energy Fuels, 2019, 3, 2642–2656.
- 47 L. Yang, Z. Wang, Y. Feng, R. Tan, Y. Zuo, R. Gao, Y. Zhao, L. Han, Z. Wang and F. Pan, Adv. Energy Mater., 2017, 7, 1701437.
- 48 O. Sheng, H. Hu, T. Liu, Z. Ju, G. Lu, Y. Liu, J. Nai, Y. Wang, W. Zhang and X. Tao, Adv. Funct. Mater., 2022, 32, 2111026.
- 49 Y. Cui, J. Wan, Y. Ye, K. Liu, L.-Y. Chou and Y. Cui, *Nano Lett.*, 2020, 20, 1686–1692.
- 50 A. Bajpai and S. Carlotti, Nanomaterials, 2019, 9, 1057.
- 51 Y. Yang, W. Yu, H. Duan, Y. Liu, X. Wang and J. Yang, *J. Polym. Res.*, 2016, 23, 188.
- 52 Y. Li, Z. Sun, D. Liu, Y. Gao, Y. Wang, H. Bu, M. Li, Y. Zhang, G. Gao and S. Ding, *J. Mater. Chem. A*, 2020, **8**, 2021–2032.
- 53 L. Gao, J. Li, J. Ju, L. Wang, J. Yan, B. Cheng, W. Kang, N. Deng and Y. Li, *Chem. Eng. J.*, 2020, 389, 124478.
- 54 Y. Ji, K. Yang, M. Liu, S. Chen, X. Liu, B. Yang, Z. Wang, W. Huang, Z. Song, S. Xue, Y. Fu, L. Yang, T. S. Miller and F. Pan, *Adv. Funct. Mater.*, 2021, 31, 2104830.
- 55 J. Wan, J. Xie, X. Kong, Z. Liu, K. Liu, F. Shi, A. Pei, H. Chen, W. Chen, J. Chen, X. Zhang, L. Zong, J. Wang, L.-Q. Chen, J. Qin and Y. Cui, *Nat. Nanotechnol.*, 2019, 14, 705–711.
- 56 A. Nishimoto, K. Agehara, N. Furuya, T. Watanabe and M. Watanabe, *Macromolecules*, 1999, **32**, 1541–1548.
- 57 G. Yang, M. L. Lehmann, S. Zhao, B. Li, S. Ge, P.-F. Cao, F. M. Delnick, A. P. Sokolov, T. Saito and J. Nanda, *Energy Storage Mater.*, 2021, 35, 431–442.
- 58 Y. Guo, X. Qu, Z. Hu, J. Zhu, W. Niu and X. Liu, *J. Mater. Chem. A*, 2021, 9, 13597–13607.
- 59 J. Shim, K. Y. Bae, H. J. Kim, J. H. Lee, D.-G. Kim, W. Y. Yoon and J.-C. Lee, *ChemSusChem*, 2015, 8, 4133–4138.
- 60 F. He, W. Tang, X. Zhang, L. Deng and J. Luo, Adv. Mater., 2021, 33, 2105329.
- 61 M. Yi, J. Li, X. Fan, M. Bai, Z. Zhang, B. Hong, Z. Zhang, G. Hu, H. Jiang and Y. Lai, *J. Mater. Chem. A*, 2021, **9**, 16787–16797.
- 62 K. Nie, X. Wang, J. Qiu, Y. Wang, Q. Yang, J. Xu, X. Yu, H. Li, X. Huang and L. Chen, ACS Energy Lett., 2020, 5, 826–832.
- 63 X. Yang, M. Jiang, X. Gao, D. Bao, Q. Sun, N. Holmes, H. Duan, S. Mukherjee, K. Adair, C. Zhao, J. Liang, W. Li, J. Li, Y. Liu, H. Huang, L. Zhang, S. Lu, Q. Lu, R. Li, C. V. Singh and X. Sun, Energy Environ. Sci., 2020, 13, 1318–1325.
- 64 H. Huo, B. Wu, T. Zhang, X. Zheng, L. Ge, T. Xu, X. Guo and X. Sun, Energy Storage Mater., 2019, 18, 59-67.
- 65 B. Chen, H. Huang, Y. Wang, Z. Shen, L. Li, Y. Wang, X. Wang, X. Li and Y. Wang, ChemElectroChem, 2022, 9, e202101277.
- 66 J. Wen, Q. Zhao, X. Jiang, G. Ji, R. Wang, G. Lu, J. Long, N. Hu and C. Xu, ACS Appl. Energy Mater., 2021, 4, 3660–3669.
- 67 C.-C. Sun, A. Yusuf, S.-W. Li, X.-L. Qi, Y. Ma and D.-Y. Wang, *Chem. Eng. J.*, 2021, 414, 128702.
- 68 C. Li, S. Zhou, L. Dai, X. Zhou, B. Zhang, L. Chen, T. Zeng, Y. Liu, Y. Tang, J. Jiang and J. Huang, J. Mater. Chem. A, 2021, 9, 24661–24669.
- 69 E. Zhao, Y. Guo, A. Zhang, H. Wang and G. Xu, *Nanoscale*, 2022, 14, 890–897.

- 70 W. Zhou, Z. Wang, Y. Pu, Y. Li, S. Xin, X. Li, J. Chen and J. B. Goodenough, Adv. Mater., 2019, 31, 1805574.
- 71 J. Liang, S. Hwang, S. Li, J. Luo, Y. Sun, Y. Zhao, Q. Sun, W. Li, M. Li, M. N. Banis, X. Li, R. Li, L. Zhang, S. Zhao, S. Lu, H. Huang, D. Su and X. Sun, *Nano Energy*, 2020, 78, 105107.
- 72 J. Liang, Y. Sun, Y. Zhao, Q. Sun, J. Luo, F. Zhao, X. Lin, X. Li, R. Li, L. Zhang, S. Lu, H. Huang and X. Sun, J. Mater. Chem. A, 2020, 8, 2769–2776.
- 73 S. Seki, Y. Kobayashi, H. Miyashiro, Y. Mita and T. Iwahori, *Chem. Mater.*, 2005, 17, 2041–2045.
- 74 J. Ma, Z. Liu, B. Chen, L. Wang, L. Yue, H. Liu, J. Zhang, Z. Liu and G. Cui, J. Electrochem. Soc., 2017, 164, A3454–A3461.
- 75 L. W. Liang, W. H. Zhang, F. Zhao, D. K. Denis, F. U. Zaman, L. R. Hou and C. Z. Yuan, *Adv. Mater. Interfaces*, 2020, 7.
- 76 S. P. Kuhn, K. Edstrom, M. Winter and I. Cekic-Laskovic, Adv. Mater. Interfaces, 2022, 9.
- 77 L. S. Li, D. M. Wang, G. J. Xu, Q. Zhou, J. Ma, J. J. Zhang, A. B. Du, Z. L. Cui, X. H. Zhou and G. L. Cui, J. Energy Chem., 2022, 65, 222.
- 78 J. Tan, X. Li, Q. Li, Z. Wang, H. Guo, G. Yan, J. Wang and G. Li, Ionics, 2022, 28, 3233–3241.
- 79 Z. Huang, W. Pang, P. Liang, Z. Jin, N. Grundish, Y. Li and C.-A. Wang, J. Mater. Chem. A, 2019, 7, 16425–16436.
- 80 Y. Xia, T. Fujieda, K. Tatsumi, P. P. Prosini and T. Sakai, J. Power Sources, 2001, 92, 234–243.
- 81 L. Han, C. Liao, X. Mu, N. Wu, Z. Xu, J. Wang, L. Song, Y. Kan and Y. Hu, *Nano Lett.*, 2021, **21**, 4447–4453.
- 82 X. Zhang, W. Guo, L. Zhou, Q. Xu and Y. Min, J. Mater. Chem. A, 2021, 9, 20530-20543.
- 83 O. Pecher, J. Carretero-Gonzalez, K. J. Griffith and C. P. Grey, *Chem. Mater.*, 2017, 29, 213–242.
- 84 J. Zheng and Y.-Y. Hu, ACS Appl. Mater. Interfaces, 2018, 10, 4113-4120.
- 85 D. Sharon, P. Bennington, M. A. Webb, C. Deng, J. J. de Pablo, S. N. Patel and P. F. Nealey, J. Am. Chem. Soc., 2021, 143, 3180-3190.
- 86 J. Yin, X. Xu, S. Jiang, H. Wu, L. Wei, Y. Li, J. He, K. Xi and Y. Gao, Chem. Eng. J., 2022, 431, 133352.
- 87 Y. Liu, Z. Ju, B. Zhang, Y. Wang, J. Nai, T. Liu and X. Tao, Acc. Chem. Res., 2021, 54, 2088–2099.
- 88 O. Sheng, J. Zheng, Z. Ju, C. Jin, Y. Wang, M. Chen, J. Nai, T. Liu, W. Zhang, Y. Liu and X. Tao, *Adv. Mater.*, 2020, 32, 2000223.
- 89 V. D. Veeraraghavan, L. Frenck, J. A. Maslyn, W. S. Loo, D. Y. Parkinson and N. P. Balsara, ACS Appl. Mater. Interfaces, 2021, 13, 27006–27018.
- X. He, S. Schmohl and H.-D. Wiemhöfer, ChemElectroChem, 2019, 6, 1166–1176.
- 91 J. Qiu, X. Liu, R. Chen, Q. Li, Y. Wang, P. Chen, L. Gan, S.-J. Lee, D. Nordlund, Y. Liu, X. Yu, X. Bai, H. Li and L. Chen, *Adv. Funct. Mater.*, 2020, 30, 1909392.
- 92 H. Huo, K. Huang, W. Luo, J. Meng, L. Zhou, Z. Deng, J. Wen, Y. Dai, Z. Huang, Y. Shen, X. Guo, X. Ji and Y. Huang, ACS Energy Lett., 2022, 7, 650–658.
- 93 B. Xu, X. Li, C. Yang, Y. Li, N. S. Grundish, P.-H. Chien, K. Dong, I. Manke, R. Fang, N. Wu, H. Xu, A. Dolocan and J. B. Goodenough, *J. Am. Chem. Soc.*, 2021, 143, 6542–6550.
- 94 B. Chen, H. Zhang, J. Xuan, G. J. Offer and H. Wang, Adv. Mater. Technol., 2020, 5, 2000555.
- L. Yang, J. Zhang, W. Xue, J. Li, R. Chen, H. Pan, X. Yu, Y. Liu, H. Li,
 L. Chen and X. Huang, Adv. Funct. Mater., 2022, 2200096.